Electron fishbone dynamics studies in tokamaks using the XHMGC code

V. Fusco[1], G. Vlad[1], S. Briguglio[1], G. Fogaccia[1]

[1]ENEA for EUROfusion, Frascati, (Rome) Italy

E-mail contact of main author: valeria.fusco@enea.it

Abstract. The electron fishbone modes are internal kink instabilities induced by suprathermal electrons. Ion fishbones were first observed experimentally (PDX) [1], opening the path to full theoretical understanding of these phenomena [4]. Stimulated by experimental evidence of electron fishbones (DIII-D, Compass-D, FTU, Tore-Supra), theoretical analysis has also been extended to the case of modes excited by fast electrons [5]. It is well known that additional heating of a plasma produces suprathermal particles which, under certain conditions, could destabilize symmetry breaking modes. Moreover, the dynamics of suprathermal electrons in present days experiments has analogies to that of alpha particles in future burning plasma devices; and resonant excitation by fast electron precession resonance may provide a good test bed for understanding the similar mechanism induced by fusion alphas. For these reasons, it is important to get insights into the underlying physics processes involved in these phenomena. In this work, numerical simulations with the HMGC code [6] are systematically carried out in tokamak equilibria. On the one side, theoretical and experimental results are confirmed, while, on the other side, numerical simulations give a deeper insight into the e-fishbones dynamics. Linear and non-linear studies of e-fishbone instability have been performed for standard (peaked on-axis) [7] and inverted (peaked off-axis) suprathermal electron density profile, with moderately hollow q-profile. It is worth noting that the two situations are significantly different in terms of the characteristic resonance frequency as well as the fraction of suprathermal particles involved in the destabilization of the mode, confirming theoretical expectations. The study of e-fishbone nonlinear saturation mechanisms uses the test particle Hamiltonian method (TPHM) package [8], illuminating the complicate and unexplored dynamics of these modes.

1. Introduction

The electron fishbone modes are internal kink instabilities induced by fast electrons (suprathermal electrons). It is known that, in tokamaks, suprathermal electrons are produced during additional heating such as lower hybrid heating or current drive (LHH, LHCD) and electron cyclotron heating or current drive (ECRH, ECCD). In the present study, the suprathermal electrons resonates with the MHD internal kink mode at the resonant frequency of the suprathermal electrons thus destabilizing symmetry breaking modes and degrading the good confinement of the energetic particles itself. Such dynamic in present days experiments has analogies to that of alpha particles in future burning plasma devices; as it is known in fact, the interaction of alpha particles with the MHD instability would happen at the toroidal precession frequency, which depends on the energy of the particles involved and not their mass. Moreover they are also characterized by a very small ratio between the resonant particle orbit width and the extension of the plasma region affected by the radial kink displacement; the same feature would be found for alpha particles in burning plasma devices. Thus, the resonant excitation of modes at the precession frequency, depending only on the energy of the fast particles, may provide a good test bed for understanding the similar mechanism induced by fusion alphas. For these reasons, it is important to get insights into the underlying physics processes involved in these phenomena.
Ion fishbones were first observed experimentally in PDX [1]. It was claimed that the observed mode frequency was comparable to the precession frequency of deeply trapped energetic particles. Such observation opened the path to full theoretical understanding of these phenomena [4], emphasizing that the source of instability is the radial gradient of the energetic particle distribution function. Experimental evidence of electron fishbones, instead, was found first in DIII-D [2] and Compass-D [3] and, as a consequence, theoretical analysis was extended to

the case of modes excited by fast electrons as well [5]: the same physical mechanism of ion fishbones modes was confirmed. Two peculiar cases can be distinguished: first, the suprathermal electron, namely energetic electron (EE), density profile is peaked on axis- such situation shows a negative radial gradient- and, second, the EE density profile is peaked off axis with an inverted (positive) radial gradient. To have an unstable mode [4], the following relationship has to hold $\omega_{*hot}/\omega_{\rm res} > 0$ that is the diamagnetic frequency (ω_{*hot}) and the resonance frequency ($\omega_{\rm res}$) must have the same sign. It means that the resonance frequency of the particles has the electron diamagnetic direction for the peaked on axis profile and the reversed one, that is ion diamagnetic direction, in the other case. Deeply trapped particles drive the mode for the peaked on axis profiles because they are able to give a mode frequency in the electron diamagnetic direction, whilst, for the peaked off axis case, the particles contributing to the mode are the barely trapped/ circulating ones which, indeed, give a frequency rotating in the ion diamagnetic direction [5].
Previous work [7] has numerically analyzed the case of EE with a peaked on axis density profile. It was the first numerical experiment involving electrons that poses the numerical challenge of properly handing the extremely fast parallel electron motion along equilibrium magnetic field lines. A peaked on axis case was chosen to simplify the physical processes involved in the simulations thus avoiding the mixture of circulating and magnetically trapped particles; at the same time the work confirmed the same physical processes supposed for ion fishbones.
In this paper linear and non-linear studies of e-fishbone instability have been performed and compared for both standard (peaked on-axis) and inverted (peaked off-axis) EE density profile, with moderately hollow q-profile. As already underlined, the two situations are significantly different in terms of the characteristic resonance frequency as well as the fraction of EE involved in the destabilization of the mode; on the one side, theoretical and experimental results are confirmed, while, on the other side, numerical simulations give a deeper insight into the e-fishbones dynamics. Numerical simulations with the HMGC code are systematically carried out in tokamak equilibria whilst the study of e-fishbone nonlinear saturation mechanism uses the test particle Hamiltonian method (TPHM) package [8].

2. Numerical simulations set up

The HMGC code is based on a hybrid MHD-gyrokinetic model [6]. It was originally developed at the Frascati ENEA laboratories and it has been already applied successfully to studies of energetic particles driven modes (such as TAE -toroidal Alven eigenmodes- or EPMs -energetic particles modes) and to existing devices (JT-60, DIII-D). In the code, the thermal plasma is described by a $O(\epsilon^3)$ reduced-MHD equations in the zero pressure limit with circular shifted magnetic surfaces whilst the energetic particles dynamic is described by Vlasov equations in the drift kinetic limit with a particles-in-cell technique. For simplicity, the analysis is restricted to the case in which fluid non linearities are neglected whilst the particles are treated non-linearly. Simulations are self-consistent because energetic particles contribute to MHD equations through the divergence of the pressure tensor.
The code is able to evolve up to three independent kinetic populations assuming different equilibrium distribution functions (for example bulk ions, energetic ions and/or electrons). In this work a bulk ion (deuterium) and an EE populations are considered. The EE temperature radial profile is constant with $T_{e0} = 50keV$; the bulk ion population temperature is $T_i/T_{i0} = (1 - \psi)$ with $T_{i0} = 2keV$ the on axis value. Here ψ is the normalized poloidal flux ranging from $\psi = 0$ on axis and $\psi = 1$ at the plasma boundary. The on axis magnetic field is $B = 5.4T$. The normalized Larmor radius of the EE is $\rho_e/a = 3.5 \times 10^{-4}$ and of thermal ions $\rho_i/a = 4.27 \times 10^{-3}$

where a is the minor plasma radius. The inverse aspect ratio of the tokamak is $\epsilon = 0.1$. With these characteristics, the normalized EE thermal velocity is $v_{the0}/v_{A0} \approx 12$ and the ion thermal velocity is $v_{thi0}/v_{A0} \approx 4 \times 10^{-2}$ where $v_{A0} = B/\sqrt{\mu_0 n_{i0} m_i}$ is the on axis Alfvn velocity with n_{i0} the on axis density of the bulk ions population and m_i its mass. The safety factor q profile is slightly inverted and above unity with $q \simeq 2.7$ at the external radius and $q \simeq 1$ for $r/a \simeq 0.35$. This equilibrium is used for the two cases considered, namely the peaked on-axis as well as for the peaked off-axis profile of the EE population. The two profiles are illustrated in Fig. *1.* where $n_e(\psi) = n_{e0} e^{-10\psi^2}$ for the peaked on axis case and $n_e(\psi) = n_{e0} e^{-10(\psi-0.5)^2}/e^{-10(-0.5)^2}$ for $0 < \psi < 0.5$, $n_e(\psi) = n_{e0} e^{-10(-0.5)^2}/e^{-10(-0.5)^2}$ for $\psi > 0.5$ for a peaked off axis profile; for the last case, a flat profile was chosen in the external part of the poloidal section to avoid the occurrence of modes induced in the external region of the plasma column. In fact the paper focus its attention on the internal kink mode $m = 1$, $n = 1$ where m and n are, respectively, the poloidal and toroidal mode number. The bulk ions, treated kinetically, assumes a Maxwellian distribution function; in this way the effective plasma inertia and thermal ion Landau damping are properly account [5]. Concerning the electrons, they are loaded in the code with an anisotropic distribution function given by:

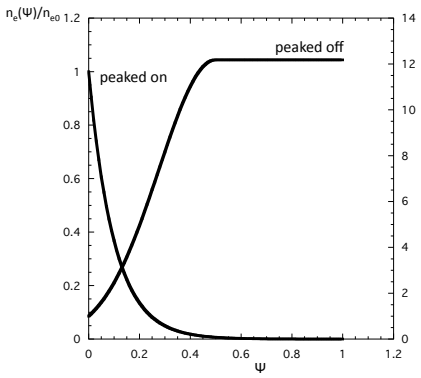

FIG. 1.: Energetic particles' density profiles.

$$f_{\text{electrons}} \equiv \left(\frac{m_e}{2\pi}\right)^{2/3} \frac{n_e(\psi)}{T_e(\psi)^{3/2}} \Theta(\alpha;\alpha_0,\Delta) e^{-E/T_e(\psi)} \tag{1}$$

$$\Theta(\alpha;\alpha_0,\Delta) \equiv \frac{4}{\Delta\sqrt{\pi}} \frac{\exp\left[-\left(\frac{\cos\alpha - \cos\alpha_0}{\Delta}\right)^2\right]}{\operatorname{erf}\left(\frac{1-\cos\alpha_0}{\Delta}\right) + \operatorname{erf}\left(\frac{1+\cos\alpha_0}{\Delta}\right)}, \tag{2}$$

$$E = \frac{1}{2} m_e u^2 + \mu\Omega_{ce}, \quad \cos\alpha \equiv \frac{u}{\sqrt{2E/m_e}}, \quad \sin^2\alpha \equiv \frac{\mu\Omega_{ce}}{E}$$

Here m_e is the electrons mass, u is the electrons parallel (to the magnetic field) velocity , $\mu = m_e u^2/2\Omega_{ce}$ the conserved magnetic momentum, α is the pitch angle, $\Omega_{ce} = -eB/(m_e c)$ the cyclotron frequency where c is the speed of light and B the local equilibrium magnetic field. $\Theta(\alpha;\alpha_0,\Delta)$ models the anisotropy of the distribution function through two parameters: the $\cos\alpha_0$ which gives the angle in the (u,μ) phase space plane where the distribution function lies and Δ which represents the width of the distribution function in the (u,μ) phase space plane. In the following analyses, it is assumed that $\cos\alpha_0 = 0$. The choice of the width Δ of the distribution function is very important and different for a peaked on axis density or a peaked off axis density. It is worth noting that the parabolas on the graphics of Fig. *2.*, represent an approximate boundary between the trapped and the circulating particles. It is known that in the case of a peaked on axis density, contributions from deeply trapped particles has to be enhanced. For this reason a thin width Δ of the distribution function is chosen thus increasing the trapped particles and decreasing the barely trapped/circulating ones. Instead, for a peaked off axis study, it is expected barely trapped/circulating particles will destabilize the mode [5]; thus a larger Δ width for the distribution function with respect to the previous case, well besides the parabolas, will be considered. Such situation is represented in Fig. *2.*, where a contour plot of the distribution function, in the (u,μ) phase space plane, is given for the two cases.

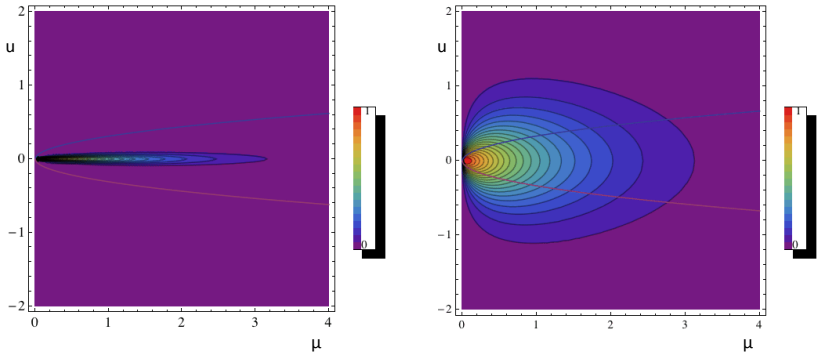

FIG. 2.: Contour plots of $\Theta(\alpha;\alpha_0,\Delta)e^{-E/T_e(\psi)}$ *. On the left hand side* $\Delta = 0.04$ *and it is used for a peaked on axis density profile; on the right hand side* $\Delta = 0.5$ *and it is used for a peaked off axis case.*

3. Linear Dynamics

When EE are excluded, no growing modes are noticeable and the considered equilibria are MHD stable. The analysis takes into account the n=1 toroidal mode number and m=1,...4 poloidal mode numbers. On the contrary, when EE are turned on, with a proper choice of their density profile (Fig. *1.*), unstable modes are observed, experiencing a linear growth phase and a subsequent saturation state. This is represented in Fig. *3.*. For the peaked on axis density,

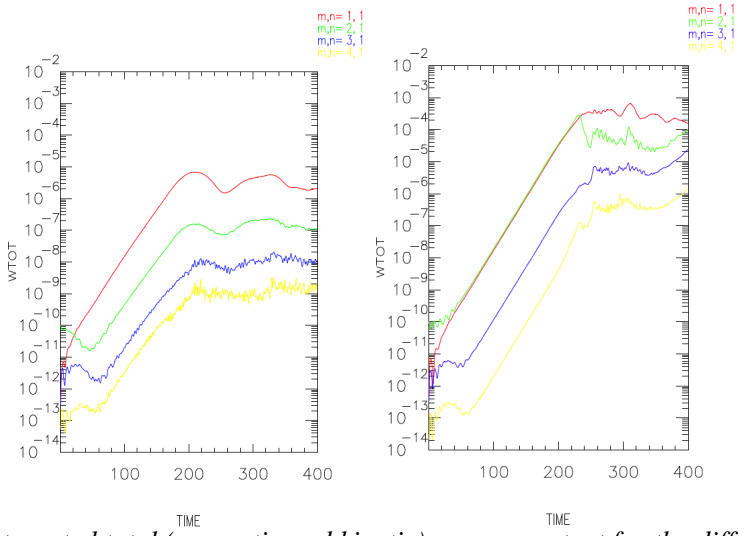

FIG. 3.: Volume integrated total (magnetic and kinetic) energy content for the different Fourier components used in the simulation for a peaked on axis density (left hand side) and for a peaked off axis density (right hand side)

$n_{e0}/n_{i0} \approx 0.025$ has been chosen, whilst the peaked off axis one uses $n_{e0}/n_{i0} \approx 0.018$, where n_{i0} is the bulk ion density value on axis. For both cases, the EE induces an $(m,n) = (1,1)$ internal kink mode, that is the electron fishbone, with a growth rate $\gamma = 0.035$ for the peaked on axis density and a growth rate $\gamma = 0.038$ for the peaked off axis case, Fig. *3.*. The mode lies, in the frequency plane $(\omega/\omega_{A0}\ ,\ r/a)$, around the $q \approx 1$ rational surface (Fig. *4.*) and it exhibits a mode frequency $\omega/\omega_{A0} = -0.05$ and $\omega/\omega_{A0} = +0.012$ for the peaked on axis and peaked off axis case, respectively; ω_{A0} is the Alfven frequency. Note that the mode frequencies are obtained from the code using a standard FFT; this assumption is opposite to the one generally considered in analytical papers.

The two scenario, are quite different because of the opposite sign of the radial density gradient; thus the mode is expected to rotate in the bulk electron diamagnetic direction in the peaked on axis case whilst it rotates in the opposite direction, that is, in the bulk ion diamagnetic direction,

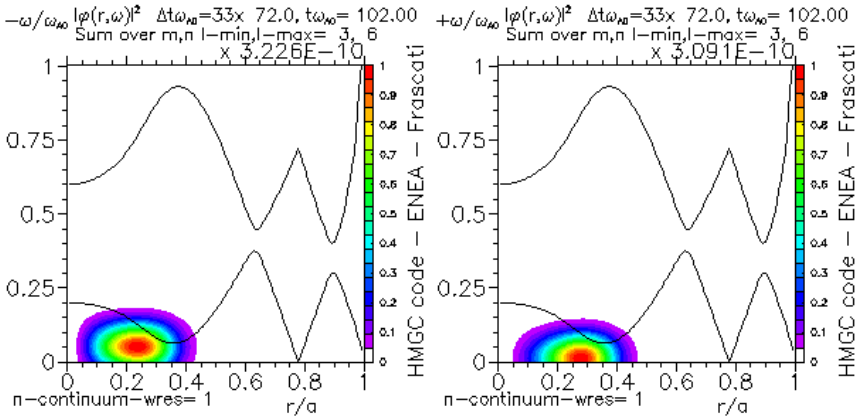

FIG. 4.: *Power spectrum of the electrostatic field at a chosen time $t\omega_{A0}$, during the linear dynamics, for a peaked on axis density (left hand side) and for a peaked off axis density (right hand side). Solid curves show the upper and lower shear Alfven continua.*

in the peaked off axis one. The energy exchange between particles and the mode should be quite different, as well. In fact for a standard (on axis) gradient, deeply trapped particles are expected, from theory, to destabilize the mode, whilst barely trapped/circulating particles play the role in the case of a peaked off axis density. As can be seen from Fig. *5.*, on the left hand side (Fig. *5.*a) and Fig. *5.*c)), the mode is represented in the poloidal plane and the arrow represents the direction of rotation which is counterclockwise for peaked on axis profile and clockwise for peaked off axis profile; on the right hand side (Fig. *5.*b) and Fig. *5.*d)), the exchange of energy between the mode and the EE is shown. The red colors represents the maximum amplitude exchange, thus deeply trapped are visible for the peaked on axis case whilst barely trapped/circulating particles are evident for the peaked off axis profiles, being the parabolas an approximate estimation of the boundary between trapped (inner area) and circulating particles (outer area). Such statements are furthermore confirmed in the following numerical experiment. In fact the contribution of deeply trapped particles can be artificially turned off in the peaked on axis simulation; as the system becomes stable, one can claim that deeply trapped EE actually drive the mode. Moreover, if barely trapped/circulating particles are turned off for the peaked off axis profiles, the mode becomes stable assuring that, in this case, energetic barely trapped/circulating electrons cause the mode to grow. For all these reasons, the choice of the distribution function anisotropy is very important as well. In fact changing the width Δ of the distribution function, the portion of particles, involved in the drive of the

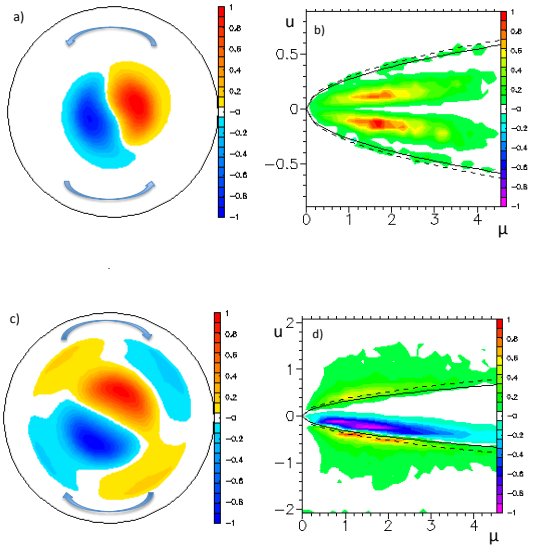

FIG. 5.: *On the left hand side, poloidal structure of the EE driven mode (electrostatic component of the fluctuating electromagnetic field) for peaked on axis density a) and peaked off axis density c). On the right hand side, power exchange between EE and the mode for peaked on axis density b) and peaked off axis density d) at the radial position of the maximum power exchange.*

mode, changes, including initially deeply trapped particles (small Δ) and then also circulating and well circulating particles(large Δ) (as already depicted in Fig.*2.*). In the case of peaked on axis density, the situation is depicted in Fig. *6.* (left hand side) where the growth rate is represented vs Δ. When Δ deviates from the optimum value ($\Delta = 0.04$), the growth rate decreases. On the other hand, for the peaked off axis density case Fig. *6.* (right hand side), decreasing Δ means decreasing the barely trapped/circulating particles as well, thus decreasing the mode drive; on the contrary, increasing Δ means including a larger fraction of barely circultating particles, which contributes to the mode, giving an increase of the growth rate.

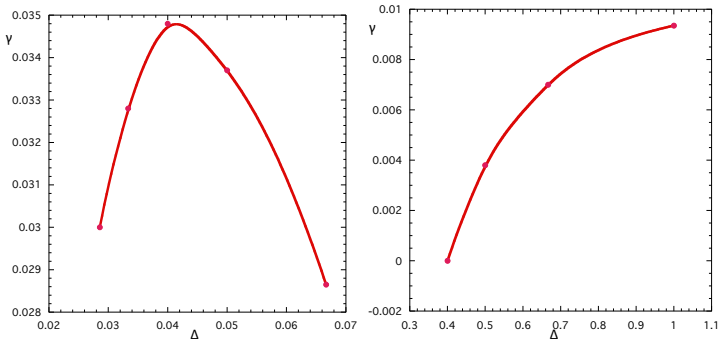

FIG. 6.: *On the left hand side, growth rate behaviour γ as a function of the width Δ for a peaked on axis density profile. On the right hand side,γ behaviour as a function of the width Δ for a peaked off axis density profile.*

4. Nonlinear Dynamics

The HMGC code can also be used to follow a set of test particles; the fields are computed and stored in a previous self consistent simulation and test particle coordinates are evolved in these fields. The advantage is that this kind of simulation allows for subsequent investigation of specific phase space regions [8]. The phase space coordinates of the test particles can be chosen such that they belong to the region where particles resonantly interact with the mode, that is, where the mode is driven unstable. To this aim, we refer the mode-particle power exchange to the μ, C velocity space, with $C \equiv \omega P_\phi - nE$ (where $P_\phi = m_e R u - e\psi/c$ is the toroidal canonical momentum). The magnetic momentum μ is a constant of motion; the quantity C is a constant as well, provided that the perturbed field is characterized by a single toroidal number n and a constant frequency ω. In the following, the analysis will be limited to a time interval in which the latter conditions are satisfied (long enough, however, to allow for the investigation of the saturation process). Once identified a point in the velocity space (μ_0, C_0), representative of the resonant phase space region to investigate, test particles are initialized with such values of μ and C, at different radial positions, in order to sample the whole region where the mode-particle dynamics takes place. Each radial coordinate r corresponds to a certain value of parallel velocity $u = u(r, \mu_0, C_0)$, and a certain resonance frequency. This frequency is given [9] by $\omega_{\rm res} = n\omega_d + [(n\bar{q} - m)\,\sigma + k]\,\omega_b$ for circulating particles; by $\omega_{\rm res} = n\omega_d + k\omega_b$, for trapped particles. Here, ω_d is the precession frequency, ω_b is the transit/bounce frequency, the integer k identifies the bounce harmonics, $\sigma = sign(u)$, and the average safety factor $\bar{q}$ is calculated as $\bar{q} \propto \oint q d\theta$ over the particles orbit. Note that, the constancy of μ and C make the time evolution of the specific resonance considered self contained: none of the considered particles can leave or get the surface $(\mu = \mu_0, C = C_0)$, and no gradients orthogonal to such surface can have relevance in the mode-particle dynamics.
In this paper, the analysis of the non linear evolution is carried on with reference to an equilibrium slightly different from that adopted for the linear stability analysis of the previous section

; namely, while the safety factor still shows a moderately hollow profile around $r/a = 0.35$, it reaches the value $q \simeq 5$ at the external radius. In this way the resulting mode frequency is larger, in magnitude, for both peaked-on-axis and peaked-off-axis EE radial profiles ($\omega/\omega_A = -0.06$ and $\omega/\omega_A = 0.043$, respectively), allowing for an easier analysis of the mode evolution (the mode period observed in the previous section is so long that many particle properties would be difficult to investigate in the nonlinear phase). All the important linear-phase features previously discussed, such as mode rotation direction and radial localization, are however confirmed in this new case.
In Fig. *7.* mode frequency and the resonance frequency, calculated numerically from test particle evolution, are compared for a peaked-on-axis density (left) and a peaked-off-axis one (right), during the linear phase: plots show that power exchange is peaked around the radial position where the resonance frequency crosses mode frequency. The hamiltonian mapping technique

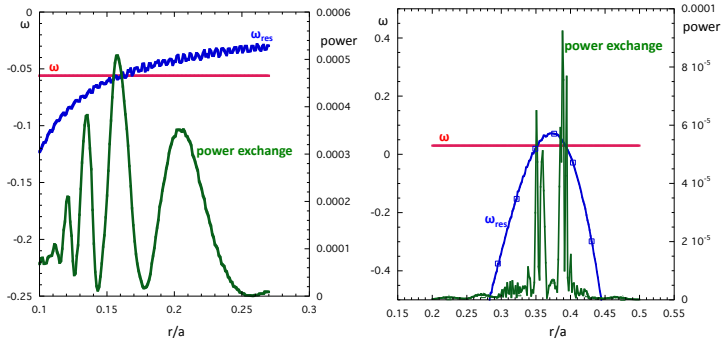

FIG. 7.: Comparison between mode frequency ω and the resonance frequency $\omega_{\rm res}$ computed for the test particle set for a peaked-on-axis (left) and peaked-off-axis (right) EE density profiles. The mode-particle power exchange profile is also represented.

[8] consists in mapping the test particles onto a (P_ϕ, Θ) Poincaré plane, with Θ being the wave-phase seen by the particle. Particle quantities are gathered each time the particle complete a full trapped or transit orbit, crossing the equatorial plane at its (radially) outmost $\theta = 0$ position.
For unperturbed motion, P_ϕ would be a constant, and particles would be represented, in the Poincaré plane, by markers drifting along Θ, in the positive (negative) direction for ω greater (smaller) than $\omega_{\rm res}$. Particles with $\omega = \omega_{\rm res}$ are represented by fixed markers at $P_\phi = P_{\phi{\rm res}}$. In the presence of a perturbed field, particles are displaced in P_ϕ, due, e.g., to the $E \times B$ drift. Even a perfectly resonant particle is brought out of resonance, and it starts to drift. As the wave phase seen by the particle is such that the perturbed field is seen with inverted sign, the P_ϕ excursion is inverted, and the particle crosses the $P_\phi = P_{\phi{\rm res}}$ line. Phase drift is then inverted too, and the process tends to yield a (neary) closed orbit: such particles are captured in the wave. Particles starting far from the resonance have their orbit in the Poincaré plane only undulated by the P_ϕ displacement, maintaining a drifting (passing) character. The P_ϕ extension of the capture region increases with increasing field amplitude.
In this study, two kind of plots are used: in the first one, markers are coloured according to particle instantaneous power-transfer rate; in the second one, according to their initial P_ϕ value. Fig. *8.* shows the localization in the (P_ϕ, Θ) plane of the maximum power exchange for the peaked-on-axis and peaked-off-axis EE density profile. It is worth noting that in the peaked-off-axis case, two resonances, corresponding to $P_{\phi res} \simeq 130$ and $P_{\phi{\rm res}} \simeq 160$, are apparent (this is shown in Fig. *7.* as well, where the particle resonance intercept the mode frequency at two radial positions). In the peaked-on-axis case, a single resonance is instead observed, at $P_{\phi res} \simeq 15$. The $P_{\phi res}$ localization is taken into account in the second kind of plot by choosing the (constant) colour of each marker on the basis of the particle initial P_ϕ coordinate, relative to $P_{\phi res}$, as shown in Fig. *9.* (single resonance, two colours) and Fig. *10.* (double resonance, three

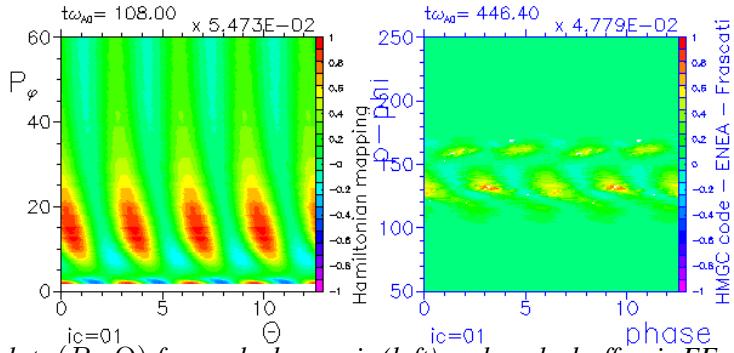

FIG. 8.: Poincare plots (P_ϕ, Θ) for peaked-on-axis (left) and peaked-off-axis EE density profile (right). Each test particle is coloured according to its rate of power transfer to the mode.

colours).
In the peaked-on-axis case (Fig. *9.*), we observe the P_ϕ elongation of the red structure formed by particles born with $P_\phi < P_{\phi res}$ and displaced by the perturbed field. This feature can be easily interpreted from Fig.*7.*(left): because of the flat nature of ω_{res}, for $r > r_{res}$, particles have to undergo a radial displacement (that is a P_ϕ displacement) before getting a significant value of $|\omega - \omega_{res}|$ and the corresponding Θ drift. The peaked-off-axis case (Fig. *10.*) is instead char-

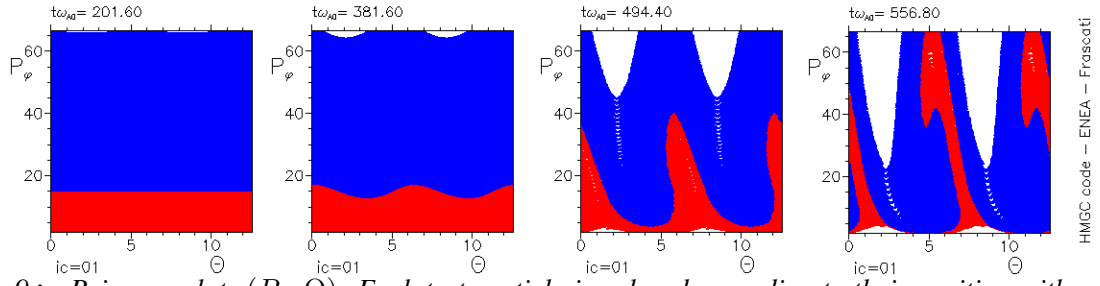

FIG. 9.: Poincare plots (P_ϕ, Θ). Each test particle is colored according to their position with respect to the $P_{\phi res}$ at $t = 0$. Blue when $P_\phi > P_{\phi res}$ and red otherwise. In the graphic the plots are shown at different times.

acterized by sharper variation of ω_{res} around each of the two resonances. This feature allows for the formation of two captured-particle regions (cf. the frame corresponding to $(t\omega_A = 559)$. As the mode amplitude further increases $(t\omega_A = 664)$, the two regions partially overlap: some of the particles born out of the outer resonance (yellow) enter the region of the inner resonance (originally red), and viceversa. As a conclusion, from the previous plots, it can be noticed

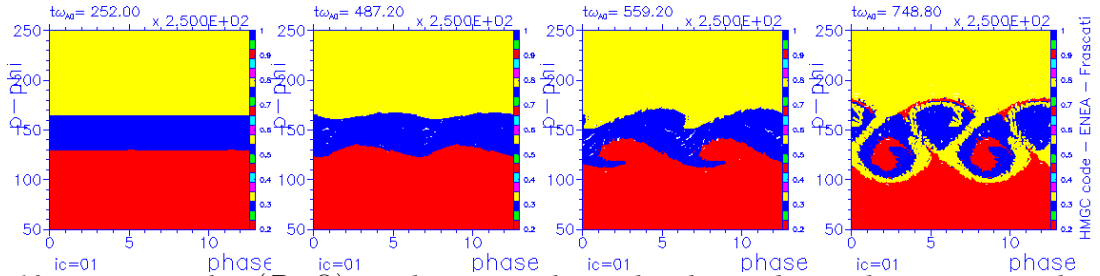

FIG. 10.: Poincare plots (P_ϕ, Θ). Each test particle is colored according to their position with respect to the $P_{\phi res}$. Yellow when $P_\phi > P_{\phi res2}$, blue when $P_{\phi res1} < P_\phi < P_{\phi res2}$ and red when $P_\phi < P_{\phi res1}$. In the graphic the plots are shown at different times.

that during the non linear dynamics, mutually penetrating structures are revealed; it means that different density portions of the energetic particle population exchange their radial position, yielding a density flattening. This phenomena is shown in Fig. *11.* for peaked-on-axis (left)

and peaked-off-axis (right) density profile. Density flattening, reducing the free energy source, contributes to the mode saturation.

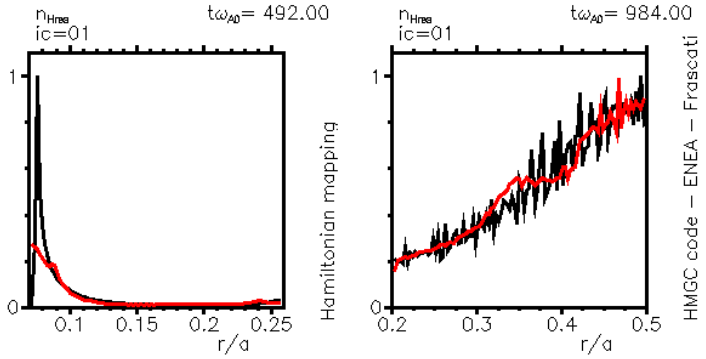

FIG. 11.: *Density flattening for the peaked on axis (left) and peaked off axis profile (right).*

Acknowledgements.
The authors would like to thank Fulvio Zonca for many helpful and interesting discussions.
The computing resources and the related technical support used for this work have been provided by CRESCO/ENEAGRID High Performance Computing infrastructure and its staff. This work has been carried out within the framework of the EUROfusion Consortium and has received funding from the Euratom research and training programme 2014-2018 under grant agreement No 633053. The views and opinions expressed herein do not necessarily reflect those of the European Commission.

References

[1] McGuire K., et al. *Phys. Rev. Lett.*, **50**, (1983) 891-5
[2] M. Wong, et al., *Phys. Rev. Lett.*, **85**, (2000) 996.
[3] K.L. Valovic, et al., *Nuc. Fusion*, **40**, (2000) 1569.
[4] Chen L., White R.B. and Rosenbluth M.N., et al. *Phys. Rev. Lett.*, **52**, (1984) 1122-5
[5] Zonca F., et al., *Nucl. Fusion*, **47**, (2007) 1588.
[6] Briguglio S., et al., *Phys. Plasmas*, **2**, (1995) 3711.
[7] Vlad G., et al., *Nucl. Fusion*, **53**, (2013) 083008.
[8] Briguglio S., et al., *Phys. Plasmas* , **21**, (2014) 112301.
[9] Zonca F., et al., *Rev. Mod. Phys.* , (2014) submitted.